Estuarine, Coastal and Shelf Science (2002) **54,** 453–472
doi:10.1006/ecss.2000.0658, available online at http://www.idealibrary.com on IDEAL®

Modelling the Danube-influenced North-western Continental Shelf of the Black Sea. I: Hydrodynamical Processes Simulated by 3-D and Box Models

J. M. Beckers[a,*], M. Gregoire[a], J. C. J. Nihoul[a], E. Stanev[b], J. Staneva[b] and C. Lancelot[c]

[a]*Université de Liège, GHER, Sart-Tilman B5, B-4000, Liège, Belgium*
[b]*University of Sofia, Department of Meteorology and Oceanography, 5 James Bourchier Str., BG-1126, Sofia, Bulgaria*
[c]*Ecologie des Systèmes Aquatiques, Université Libre de Bruxelles, CP 221, Campus Plaine, Bd. du Triomphe, B-1050, Bruxelles, Belgium*

Received September 1998 and accepted in revised form September 1999

A hydrodynamical modelling of the Black Sea is presented using the GHER 3-D primitive equation model. Results of a very high resolution model with 5 km grid size are analysed and the dominant features of general circulation in the Black Sea are highlighted. Compared with a coarse resolution model, forced with the same climatic monthly averaged atmospheric data, the high resolution model exhibits stronger variability, including frontal structures and coastal upwellings induced by baroclinic instabilities, in particular along the Turkish coast. A comparison of the shelf-open sea exchanges, with particular focus on the cold intermediate waters, shows that both models lead to a replenishment of the CIL in the basin interior by cold waters formed on the shelf.

Due to the better representation of frontal structures, the high resolution model is an appropriate candidate for coupling with a biological model. Problems of calibration, interpretation and data availability typically arise from this kind of coupled 3-D model. In order to overcome such difficulties, the results of the 3-D hydrodynamical model are used to guide the development of an integrated 0-D box model capable of achieving the objectives of projects like EROS21, where the effect of changes in the Danube inflows on the shelf ecosystem is investigated. The 0-D model is thus designed to cover this region and is obtained through integration over an appropriate variable volume. The integration procedure shows where the weaknesses of an 0-D approach might lie. Diagnoses in the 3-D model of the integral quantities show the range of uncertainty one can expect in the exchange laws of the 0-D model.

Keywords: hydrodynamical 3-D model; box model; Black Sea; Danube

Introduction

The present modelling is an attempt to provide a mathematical modelling framework in which certain hypotheses of the EROS21 project can be tested: e.g. whether ecosystem damage and the collapse of fisheries observed in the late 1980s–early 1990s in the Black Sea are due to—changes in the hydrologic regime of the Danube River caused by the 'Iron Gates'—the general increase in industry and agricultural fertilisers—the introduction of exotic species—or selective or excessive fishing. Many authors have suggested that human pressures are the reason for the profound changes observed in the Black Sea ecosystem structure. Quantifying the relative importance of these processes on the observed changes is one of the specific EROS21 objectives for the Black Sea (Lancelot *et al.*, 2002*a*), a project which focuses on the interaction between the Danube and the north-western shelf of the Black Sea. It is in this region that questions dealing with changes in riverine inputs (whether hydrological or nutrients-related) must be correctly addressed before attempting to predict the basin scale behaviour. The problem of the coastal area acting as a buffer zone is evidently also relevant to other regions, but here we focus on the specific aspects of the Danube influence.

Since it is difficult to calibrate and validate a fully coupled 3-D biological–hydrodynamical model capable of dealing with changes in the ecosystem structure, the following strategy is applied: generally, the choice of an adequate biological model to be coupled with a 3-D hydrodynamical model is not inconsequential and takes into account questions like data availability, the number of calibration parameters, local specifities and mathematical/numerical complexity [e.g. Nihoul (1998)]. A

*Corresponding author. E-mail: JM.Beckers@ulg.ac.be

0272–7714/02/030453+20 $35.00/0

simplified hydrodynamical model allows for a wide range of biological models to be tested and calibrated. We will therefore start by developing a fully 3-D model, on which diagnoses are performed so that a simpler local 0-D hydrodynamical model can be forced on a sound basis.

The purpose of the present paper is thus first of all to show the performance of the 3-D models by simulating the general circulation of the Black Sea. Secondly, it aims to use the model's results to calculate simplified exchange laws for a box integrated model of Danube-influenced waters.

In the second paper (Lancelot *et al.*, 2002*b*), these exchange parameters are used in the 0-D box coupled to the BIOGEN biological model, and the sensitivity of the model response to the input parameters is assessed.

The general circulation with its cyclonic pattern has already been studied by a series of authors (e.g. Stanev, 1988, 1990; Ozsoy *et al.*, 1993; Oguz *et al.*, 1995; Oguz & Malanotte-Rizzoli, 1996). Of course, their results demonstrate that the shelf's dynamics are directly influenced by the so-called Rim current. This current flows cyclonically around the Black Sea and from the east along the northern coast and the shelf break, with some excursions onto the shelf. However, no diagnoses for a box model at the Danube river mouth have been calculated yet.

Classical simulations of the general circulation use relatively coarse resolution models (with a grid size comparable to or larger than the Rossby radius of deformation). In such models, the strong, non-linear behaviour of regions influenced by the river is unlikely to be well accounted for. We therefore implemented a high resolution model on the whole basin. This allowed a direct comparison with the standard low-resolution model and also helps design an appropriate nesting technique (Noméerange & Beckers, 1999).

But even before operating a fully nested version, a diagnosis of the high- resolution model is performed to produce information for a 0-D coupled model. This is because an integrated 0-D model can be used very easily for sensitivity studies and calibration purposes in biological models. Once these studies have been carried out and the biological model behaviour is well understood, a 3-D nested version can be implemented and used for further refinements of the modelling studies, including the analysis of spatial effects etc.

Since the development of the integrated box model is based on results of a 3-D model, we will start by describing the mathematical 3-D model. Its implementation as a coarse resolution model and a high resolution model will then be detailed. We describe results of the coarse resolution model focusing on the climatological view of the circulation. After that, the same procedure is applied to the high resolution model, focusing on processes constraining the ecosystem. A comparison of the shelf-basin exchanges in both models is then outlined. From the results of the model simulations, we show how a 0-D model can be developed. Finally, analyses of the 0-D diagnostics are presented and discussed.

Hydrodynamical model: description and implementation

Several models have already been applied to simulate general circulation in the Black Sea. Stanev (1990), give details of the performance of Bryan and Cox model, and Oguz *et al.* (1995) give details of the application of Princeton Ocean Model (POM) to the same area and Demirov (1994) shows how to use curvilinear models. Here we will analyse the results of the GHER model (Nihoul *et al.*, 1989; Beckers, 1991) whose performance is compared to the DMG-MOM model in Stanev *et al.* (2002).

The GHER 3-D mathematical model uses the free surface, the three components of the current field, temperature, salinity and turbulent kinetic energy as state variables. This quantity is used for the computation of a vertical diffusion coefficient through the classical k–l model. Numerical aspects are described in Beckers (1994), Beckers and Deleersnijder (1993), and Deleersnijder and Beckers (1992). Detailed information on its implementation for the Black Sea can be found in Stanev and Beckers (1999). The model design also allows coupling with a fully 3-D biological model on the same grid as the hydrodynamical model. General aspects of such coupling and biological modelling are described in Nihoul (1998) and Delhez (1998). On this basis, a simple 3-D biological model of the Black Sea has been implemented by Gregoire *et al.* (1997) and (1998), to test the response of biological processes to physical forcing of the large scale upwellings and frontal structures.

15 km resolution model

The coarse resolution model was set up to simulate the climatological seasonal cycle by forcing the model with climatological averages of monthly mean wind-stress fields (Sorokina, 1974), sea surface temperature and sea surface salinity. The latter two were used to prescribe Haney-type surface relaxation fluxes with relatively weak relaxation coefficients (corresponding to adaptations of a mixed layer depth of 10 m in 10 days) (Stanev & Beckers, 1998).

Monthly mean data of Altman and Kumish (1986) are used to calculate the model river discharges at

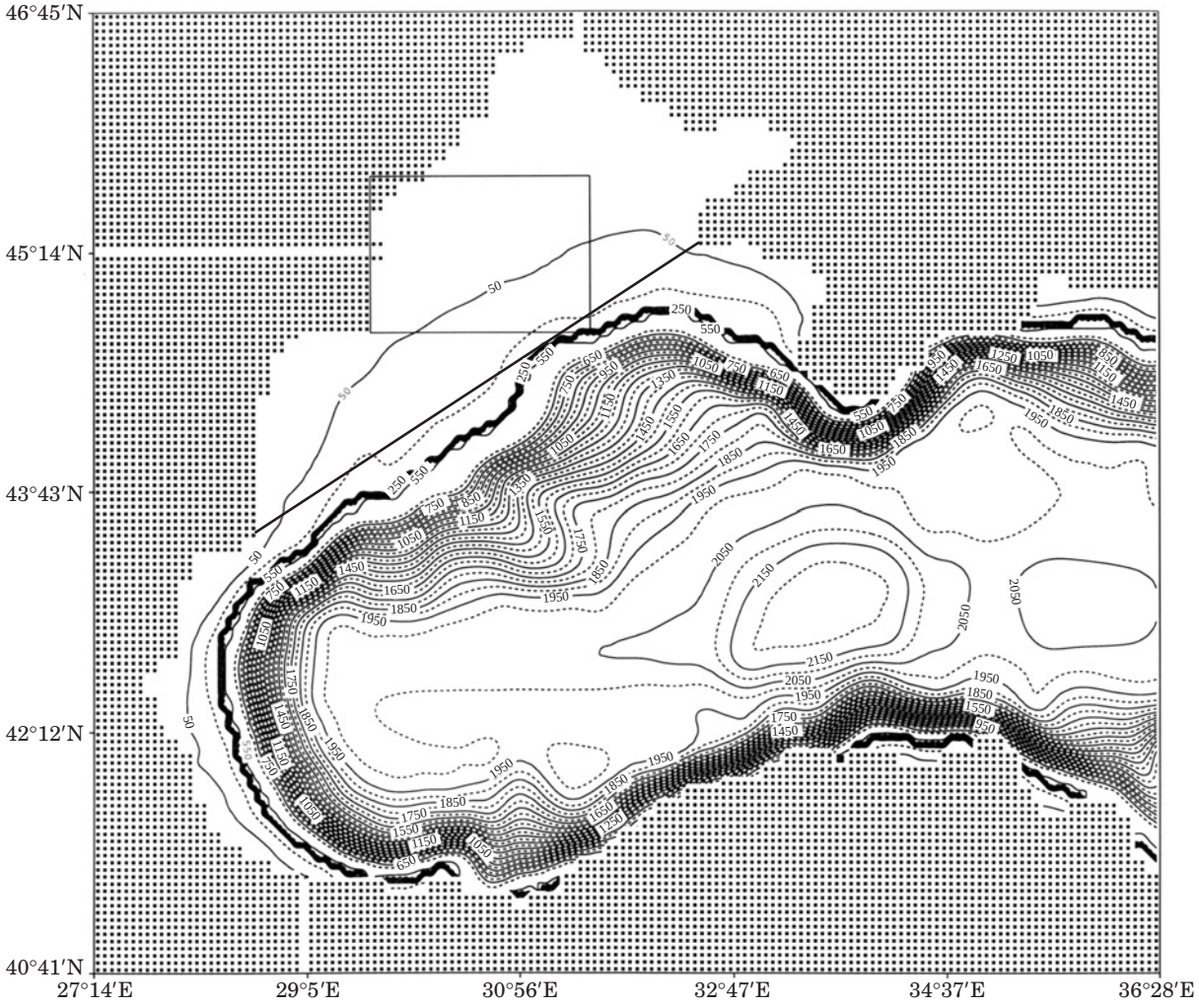

FIGURE 1. Numerical grid of the high resolution model. Only a fraction of the domain is shown, corresponding to the region of interest. The box corresponds to the region where certain diagnoses are carried out. The lines along the shelf break indicate where flux diagnoses are performed. Bathymetric contours are drawn every 50 m.

each time step using linear interpolation. River discharges at the Danube, Dnepr and Rioni are introduced by modifying boundary conditions at the solid boundary, providing the necessary lateral mass flux at the river mouth location. Smaller rivers or rivers very close to a major river were added to the three mentioned rivers (the Dnestr river contribution was for example included in the Dnepr river discharge).

In the Strait of Bosphorus, compensation of the fresh water flow at the sea surface takes place and is self-adapting to the evolution in the interior basin (see Stanev & Beckers, 1999 for details) and is a function of the sea level difference between the Mediterranean and Black Sea around the annual averaged value (Oguz *et al.*, 1990).

This model is called the coarse resolution model, though it already marginally resolves the first internal radius of deformation which is estimated to be 20 km. Here, the particular parameters set up for the model can be summarized as follows:

Horizontal resolution $\Delta x = 15$ km, vertical resolution 25 σ levels in the twofold σ coordinate change of the GHER model, horizontal sub-grid scale diffusion for tracers $\tilde{\kappa}_T = 50\ \mathrm{m^2\ s^{-1}}$, horizontal sub-grid scale viscosity for momentum $\tilde{\kappa}_u = 500\ \mathrm{m^2\ s^{-1}}$, barotropic time-step $\Delta t_{2D} = 45$ s, baroclinic time-step $\Delta t_{3D} = 1800$ s.

5 km resolution model

In this version only the grid resolution is modified (Figure 1) with the corresponding changes in the horizontal sub-grid scale parameterization and time-stepping while the forcing elements are identical to

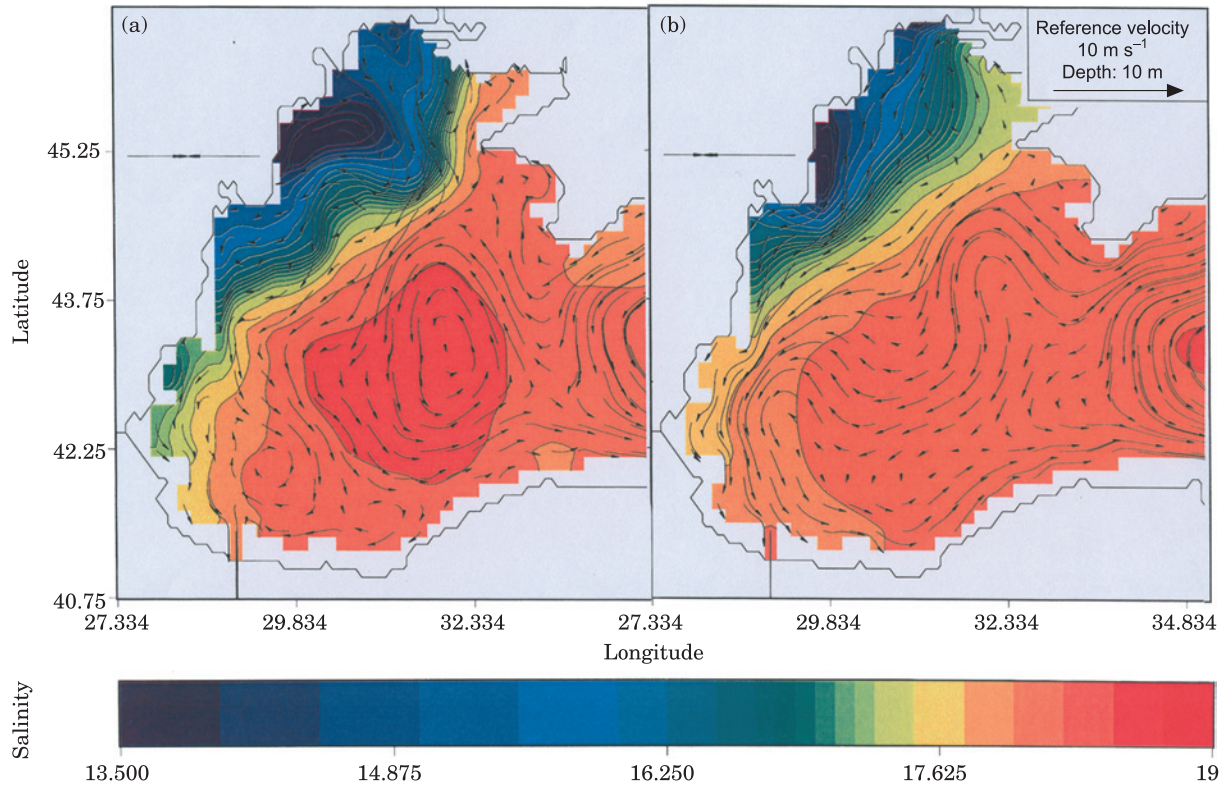

FIGURE 2. Horizontal section of currents and salinity in the coarse resolution model. (a) Spring situation corresponding to the high Danube discharge condition of May; (b) a winter situation corresponding to the low discharge condition of November.

those used for the coarse resolution model. In addition, the river input from the Danube was changed from a one grid point representation in the coarse resolution model to a three point representation in the present case. The three points correspond to the location of the three main branches of the Danube delta (St Georghe, Sulina and Chilia), which are about 30 km apart. The parameters used are horizontal resolution $\Delta x = 5$ km, vertical resolution 25 σ levels in the twofold σ co-ordinate change of the GHER model, horizontal sub-grid scale diffusion for tracers $\kappa_T = 20\ \mathrm{m^2\ s^{-1}}$, horizontal sub-grid scale viscosity for momentum $\tilde{\kappa}_u = 220\ \mathrm{m^2\ s^{-1}}$, barotropic time-step $\Delta t_{2D} = 15$ s, baroclinic time-step $\Delta t_{3D} = 1200$ s.

Both the coarse resolution and the high resolution model were spun up from a horizontally homogeneous situation for several years by the forcing which is repeated every year. Here we present some results after the spin-up.

Modelled general circulation

15 km resolution model

Previous results based on the dynamic method (Filippov, 1968), diagnostic models (Gamsakhurdiya & Sarkisyan, 1976) and primitive equation model studies (Stanev *et al.*, 1988; Oguz *et al.*, 1995) indicate that the sea surface height of the Black Sea is highest in the coastal zone and decreases as the distance from the coast increases. This reflects the general cyclonic nature of the circulation. The application of the 15 km GHER model shows that circulation on the shelf exhibits large seasonal changes. An anticyclonic eddy is formed off the Danube delta in early spring [Figure 2(a)] and widens to the east in summer (not shown). The meandering is typical of the extensions of the river plumes into the open sea (Chao & Boicourt, 1986; Hickey *et al.*, 1998).

Previous process analyses conducted for the same area proved that the scales of the front are determined by the Rossby radius of deformation (Stanev & Beckers, 1999). The modelled looping frontal pattern is supported by physical observational results recorded in July 1992 (Oguz *et al.*, 1993), although the former presented a weaker amplitude. Later in the year, the current in front of the Danube river reverses again to flow southwards [Figure 2(b)].

Theoretical analysis of the dynamics of river plumes proves that inertia tends to balance the Coriolis acceleration, which forms intrusion of open sea water

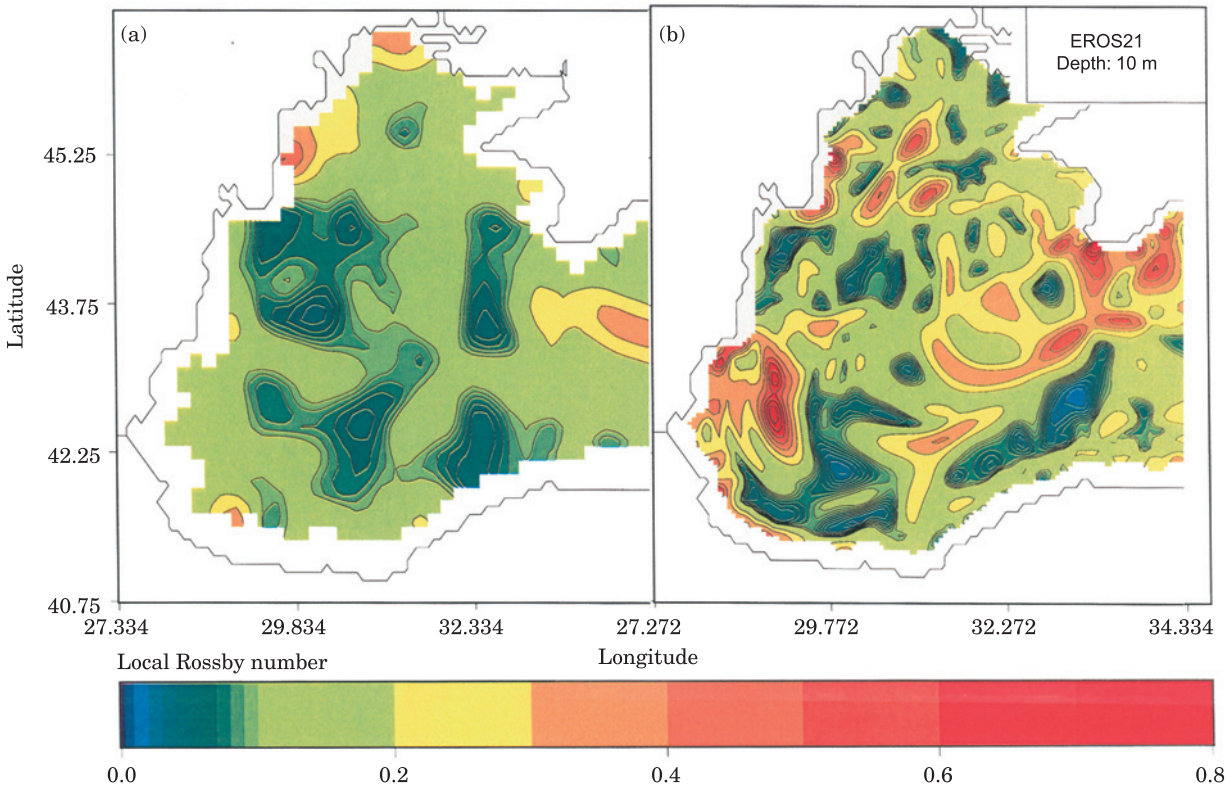

FIGURE 3. Horizontal section of the local Rossby number calculated as the ratio of the magnitude of the inertia term in the model compared to the Coriolis term in the model. Spring situation corresponding to the high discharge condition of May. (a) Coarse resolution model; (b) high resolution model.

towards the plume (Chao & Boicourt, 1986; Hickey *et al.*, 1998). Coherently, the highest values of the Rossby number are modelled in the region of the Danube and Dnepr river mouth [Figure 3(a)].

The meandering of river-influenced waters provides one mechanism of water and tracer exchanges with the open sea. A second exchange mechanism is provided by the CIW (Cold Intermediate Waters defined by temperatures below 8 °C) which are formed on the shelf and then entrained into the Cold Intermediate Layer (CIL) of the main basin. As shown in Stanev and Beckers (1998), the coarse resolution model shows the signature of these water masses below the surface layer, which compares with the observations by Oguz *et al.* (1993). The model simulates very cold waters on the shelf and then exports the CIL water by a slope current which enhances the exchange between the shelf and the open sea.

We will not analyse the results of the coarse resolution model any further (see Stanev & Beckers, 1998; Stanev *et al.*, 1999). However, with regard to the coupling with biological models, we can already indicate that the coarse resolution model has generated clear barotropic-baroclinic interactions, triggering internal waves which will determine the light environment of primary producers. Such processes are generally not resolved by coarse resolution models, but we will see that high resolution models reproduce additional processes relevant for biology.

We will come back to the issue of water and tracer exchanges with the open sea when comparing the results of the coarse resolution model with those of the high resolution model.

5 km resolution model

Figures 4 and 5 show the evolution of the surface salinity fields and the associated currents. The reversal of the current off the Danube delta is also reproduced by the high resolution model. In addition, more anticyclonic small-scale eddies are produced between the Rim current and the coast. Due to similar forcings, any change in the model results are explained by the internal dynamic of the high resolution model.

The model results (Figures 4 and 5) obviously show finer structures compared to the coarse resolution model (Figure 2). In particular, fronts are stronger and their curvature changes on smaller length scales.

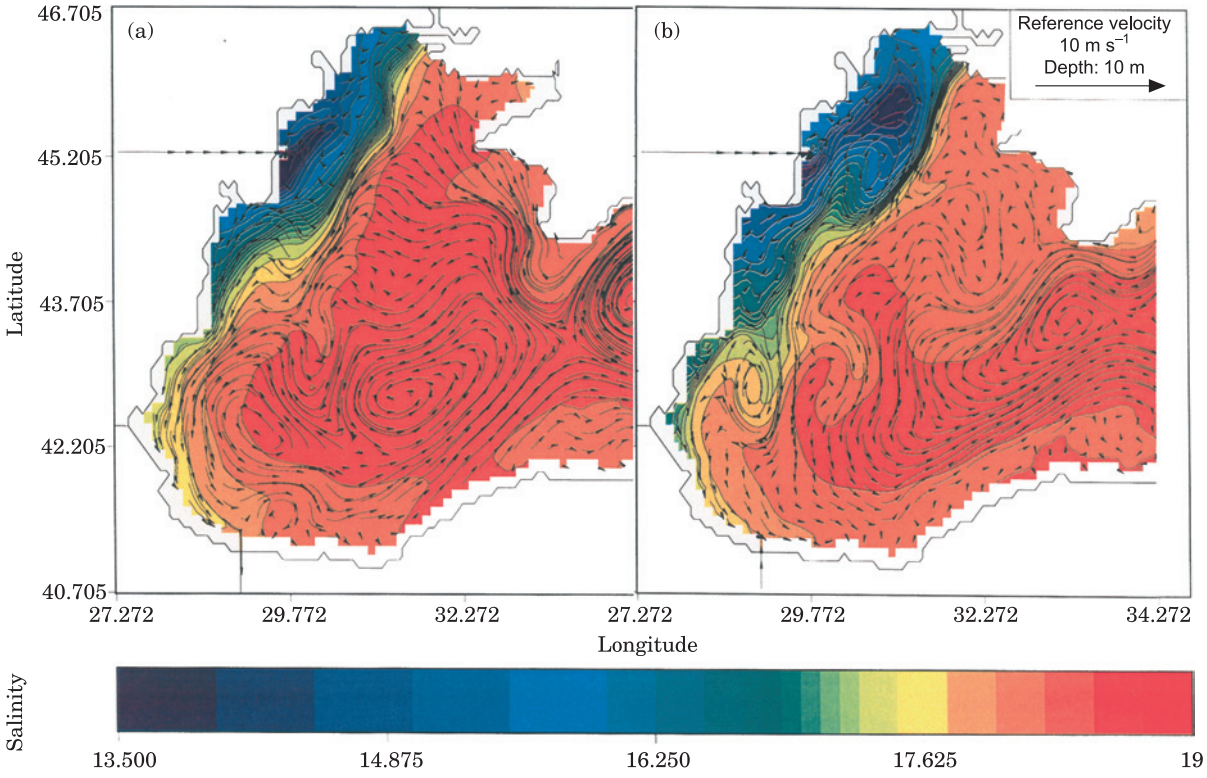

FIGURE 4. High resolution model results of salinity fields in March (a) and May (b).

This is clearly apparent in Figure 3, where the Rossby number in the high resolution model shows several locations where a non-linear effect is present. As expected, large values of the Rossby number are typical of regions with strong eddy activity. The finer description is however not the sole effect of the increased resolution. More interesting is the simulation of coastal upwellings induced by baroclinic instabilities along the Turkish coast. These were not resolved by the coarse resolution model [see Gregoire *et al.* (1998) for illustration of these effects]. This may partly be attributed to the finer representation of the bottom topography and the coastline. The coastal anticyclone at the Turkish coast around 37.5°E can be related to the presence of a topographic feature on its western side for instance (Figure 5).

The high resolution model supports the idea of the CIL water mass formation on the shelf. Figure 6 indicates that penetration of the CIL into the open sea takes place much later in the year than the moment of deep convection. The formation and evolution of cold waters, illustrated by temperature patterns (Figure 6) clearly shows that the formation of intermediate waters occurs on the shelf. The area where the cold waters penetrate into the CIL starts from the western-most point of the Crimea Peninsula and follows the isobaths, reaching the Bulgarian coast to the south. The cold water tongue splits into two branches at the end of summer: (1) west of the Crimean Peninsula, and (2) east of the Bulgarian and Romanian coasts. This splitting is caused in the model by the northern current, representing an extension of the surface loop current in the deep layers. A similar ‘ two-branch ’ configuration has been observed at a depth of 100 dbar in July 1992 (Oguz *et al.*, 1993).

In order to assess both the differences between the model behaviours and the way the CIL enters the basin from the shelf, we will now analyse the fluxes and T–S characteristics in each model. For the coarse resolution model, additional information on the inter-annual variability of these features can be found in Stanev and Beckers (1998).

Figure 7 shows the water inflow across the section along the shelf-break shown on Figure 1. Compared to the coarse resolution model, higher variability appears clearly in the high resolution model. The latter not only presents greater variability but also a higher average inflow. From the values of these inflows and the volume of the shelf waters (2×10^3 km^3) we infer shelf residence times which vary between 3 and 6 months, with an average of 4·5 months for the high resolution model.

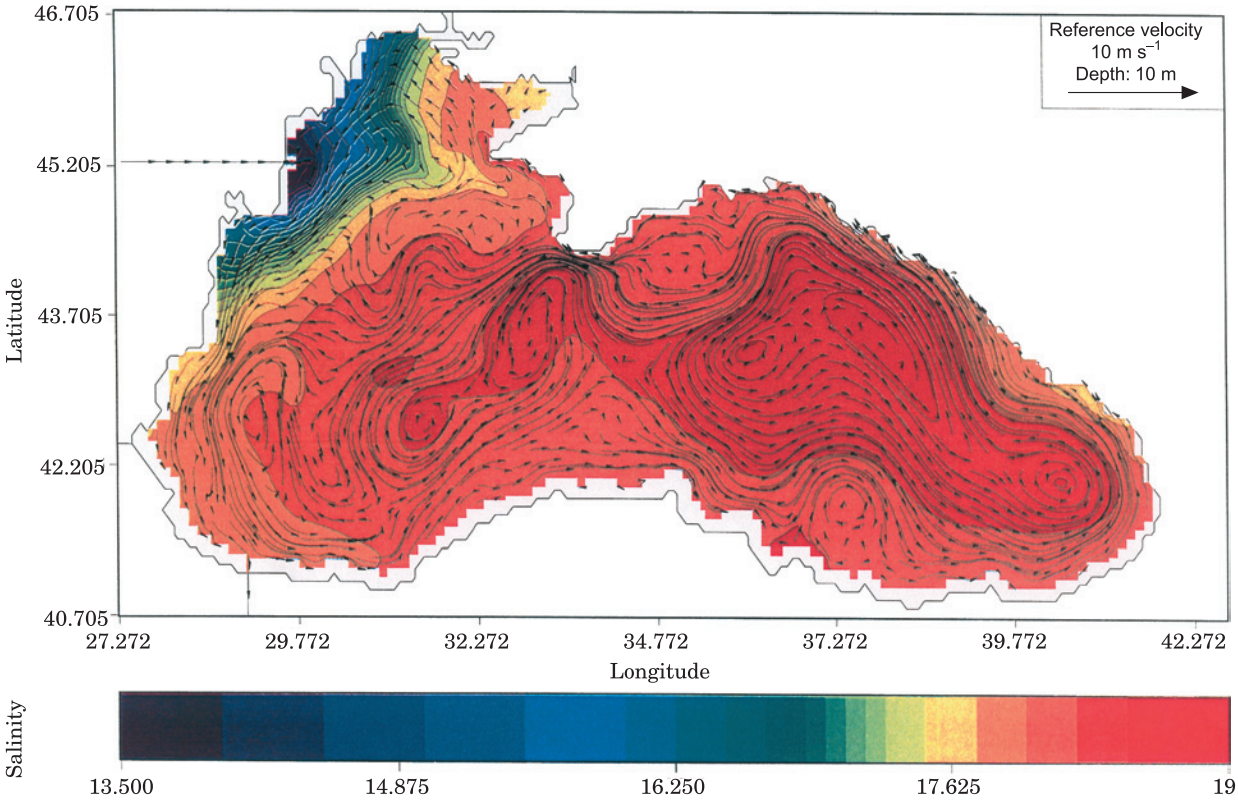

FIGURE 5. High resolution model results of salinity fields in November.

Figure 8 shows water inflows across the same section, but only the net flow of waters with temperature below 8 °C are taken into account. This thus measures the net export of CIW from the shelf to the open sea. In combination with Figure 9, it is observed that the high resolution model exports colder waters from the shelf and starts to export them to the open sea earlier than the coarse resolution model. This can be related to the enhanced circulation and transport in the high resolution model. The coarse resolution model retains the colder waters formed on the shelf for a longer time there before exporting them to the open sea in August. At this moment, compared to the high resolution model, the waters exported in the coarse resolution model are colder, because the high resolution model has already exported most of the cold waters from the shelf earlier. As the CIL has a volume of around 20 000 km^3 (Simonov & Altman, 1991), the CIW formed on the shelf would lead to a renewal time of the CIL of about 15 years, which is on the upper limit of the estimates based on hydrographic data (Simonov & Altman, 1991). In fact, CIW may also be formed in the open basin (Ivanov *et al.*, 1997), and renewal times are shorter. In the present work we focus however on the shelf-basin exchanges where the formation of CIW on the shelf is an efficient mechanism of exchange and obviously a major contribution to the overall CIW formation. Unfortunately, we cannot compare this formation rate to the formation in the open sea. This is due to our climatological forcing, which allows the complete mixing of shelf waters, but does not permit a sufficient mix of the open sea surface mixed layer down to the CIL in winter. This leads to the formation of cold waters in the open sea which are not available to fill the CIL. Also, since the actual formation rates are sensitive to the air-sea interactions (Stanev *et al.*, 1995), actual values vary from year to year. Model results of Stanev *et al.* (1995) predict renewal times of 5 to 15 years.

We close the description of the model results by analysing volumetric T–S diagrams (Figure 10). The area of dense isolines clearly suggests that most of the water in the Black Sea is confined in a rather narrow temperature interval. This sloped area indicates a mixing path between CIW and deep (large salinity) waters. The almost vertical branch of the volumetric T–S diagram (starting from the core of CIL) indicates mixing between surface (high-temperature) waters and CIW in the interior basin. The crossing of horizontal and vertical branches yields the approximate mean T–S index of intermediate water. The dispersion around this mean index illustrates the

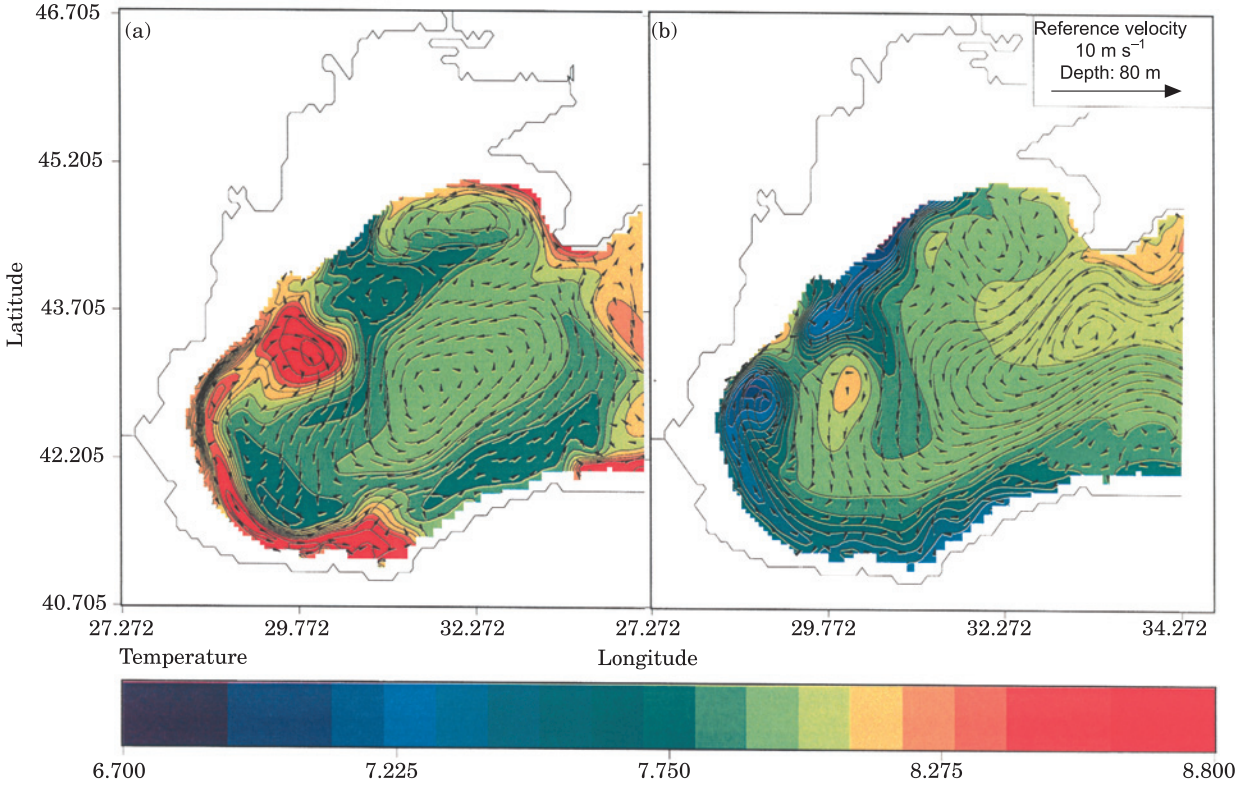

FIGURE 6. High resolution model simulation of Cold intermediate water temperature in January (a) and May (b). The newly formed water masses are not yet advected into the open sea in January but in May CIL intrusions into the open basin are simulated.

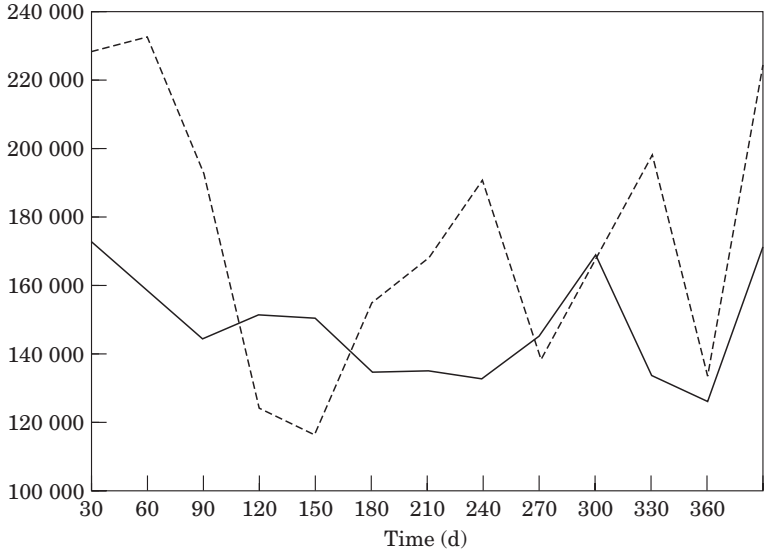

FIGURE 7. Seasonal evolution of the inflow (in $m^3\ s^{-1}$) of water onto the shelf across the section shown on Figure 1. Solid curve: results from the coarse resolution model (c.r.), dashed curve: results from the high resolution model (h.r.).

impact of transport/diffusion for the diversity of water mass characteristics. The branch in the area of lowest temperatures (close to the abscise axis) indicates the mixing of water from the shelf with intermediate water. The volumetric diagrams above can be compared with the ones of Ivanov *et al.* (1997), based

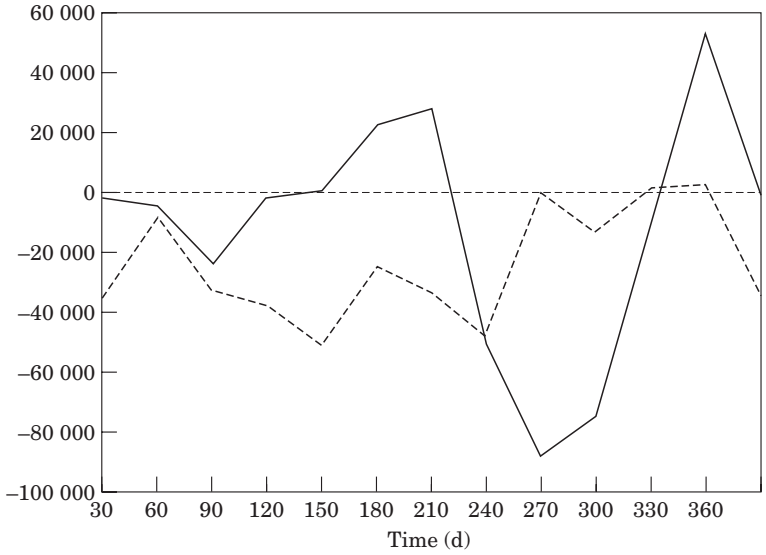

FIGURE 8. Seasonal evolution of the inflow (in $m^3 s^{-1}$) of CIL waters onto the shelf across the section shown on Figure 1. Solid curve: results from the coarse resolution model (c.r.), dashed curve: results from the high resolution model (h.r.). Negative values correspond to a flow from the shelf into the CIL.

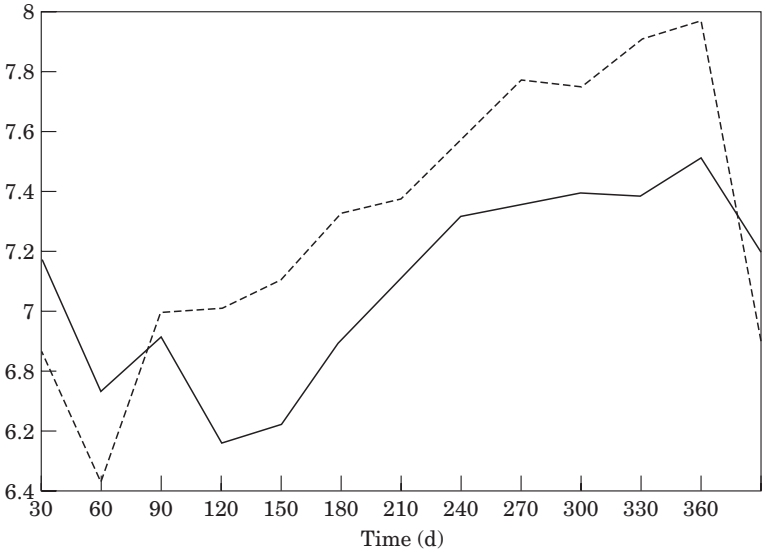

FIGURE 9. Seasonal evolution of the inflow temperature (in °) of CIL waters onto the shelf across the section shown on Figure 1. Solid curve: results from the coarse resolution model (c.r.), dashed curve: results from the high resolution model (h.r.).

on observations recorded during the multinational coordinated surveys in September 1991 and July 1992. The simulated funnel-like pattern in spring in the area of low temperatures clearly illustrates the penetration of CIW into the intermediate layers. Mixing with surrounding water tends to increase temperature and salinity, thus sinking occurs almost along the isopycnals (isolines of constant density are not superimposed on others to avoid too many lines on the plot) . The pool of extremely cold water reduces its volume from January to May, but water with temperatures below 6 °C persist until the next cooling in the coarse resolution model.

It is also interesting to observe the correlation between the low salinity patch on the shelf in May (Figure 4), CZCS images (Barale & Murray, 1995) and the results of a five-compartment biological model (Gregoire *et al.*, 1998) exemplified here by the phytoplankton response to nutrient enrichment by the Danube river (Figure 11). However, it is

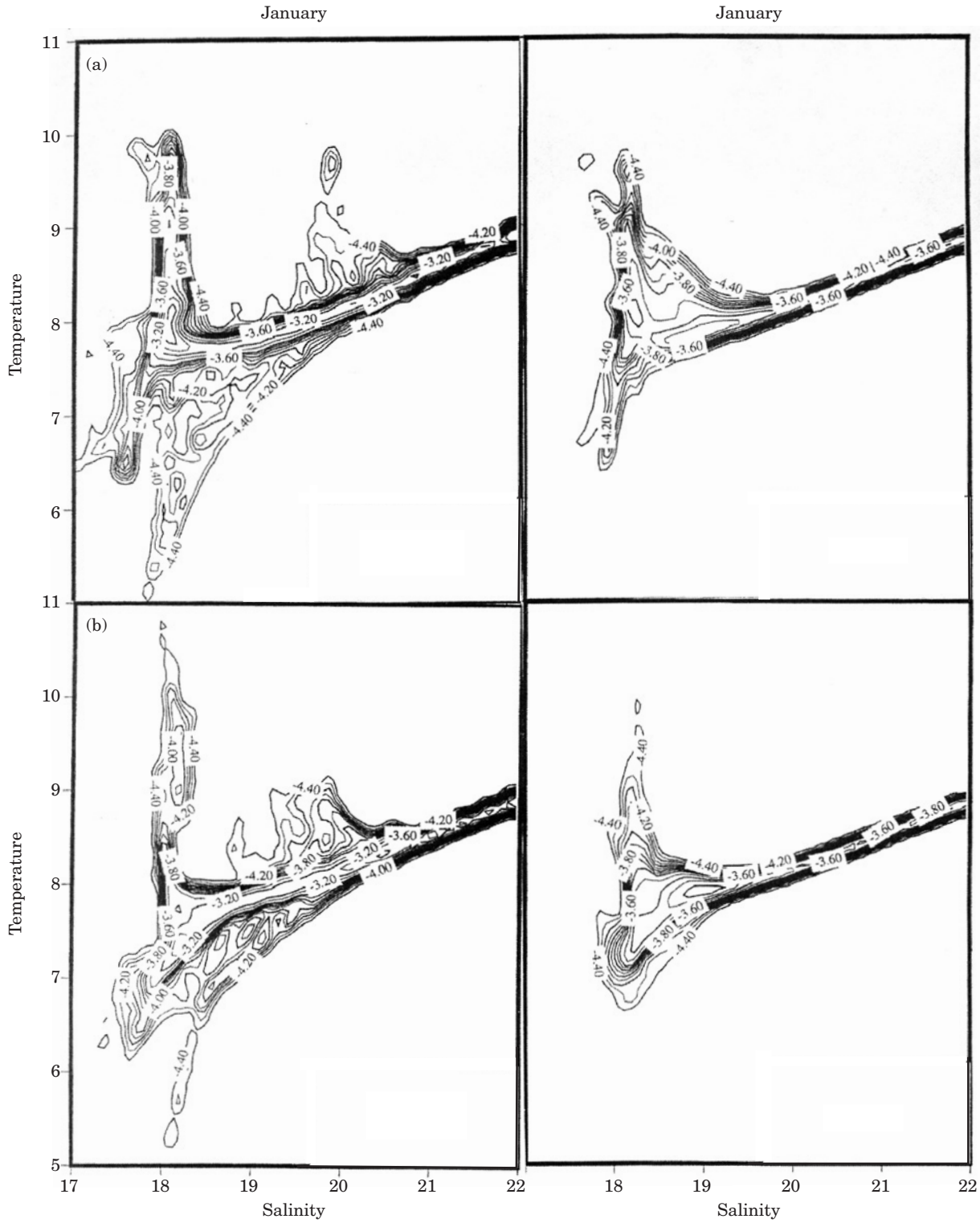

FIGURE 10. Volumetric T–S diagrams. The plots are drawn by computing the fraction of water with a T,S characteristics lying in the phase volume $[T,S] \times [T+\Delta T, S+\Delta S]$. ΔT and ΔS were chosen respectively 0·06 °C and 0·05. The fraction of water is shown on a logarithmic scale since otherwise only the homogeneous deep waters (occupying most of the volume) would be visible. (a) (top) January. Left: coarse resolution model; Right: high resolution model. (b) (below) May. Left: coarse resolution model; right high resolution model.

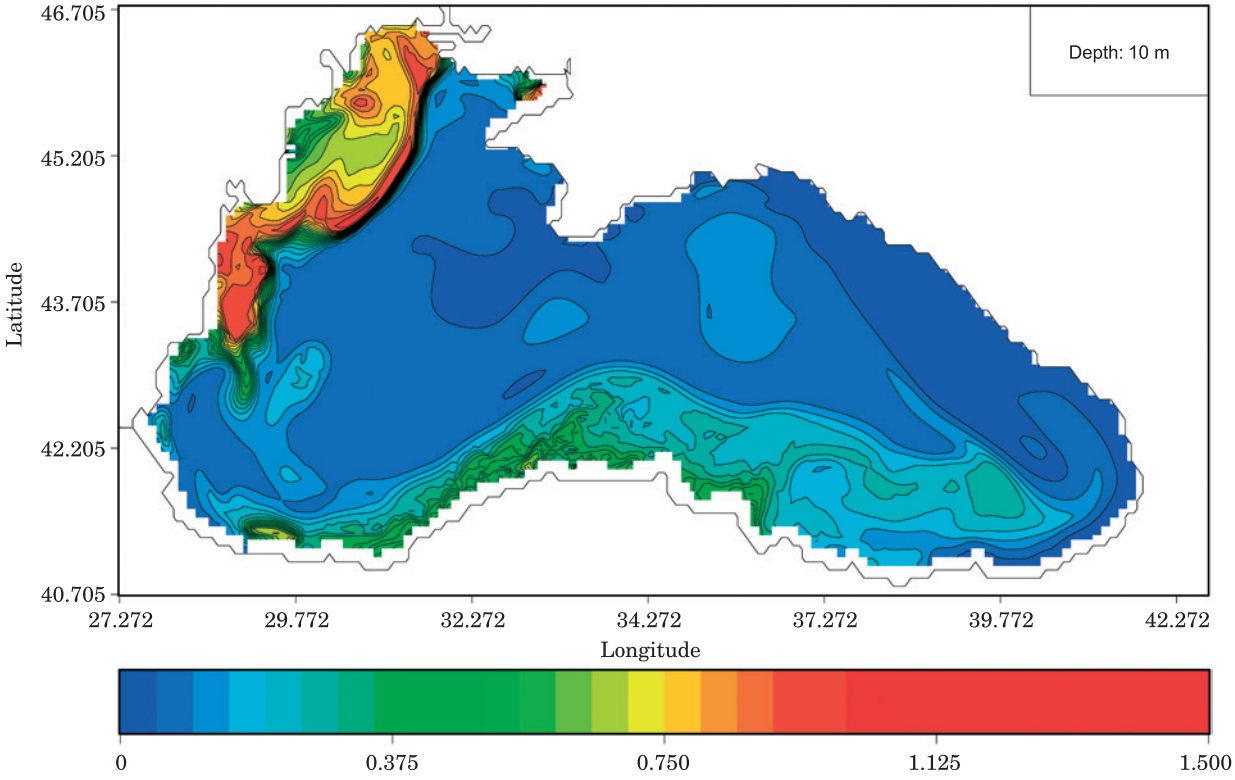

FIGURE 11. Results of a five compartment biological model coupled to the fine 3-D model. Phytoplankton concentration in May.

not the low salinity *per se* which leads to the correlation with the phytoplankton production. The relevant fact is that the water mass is discharged by the Danube river and then eventually trapped in an anticyclonic gyre. In this case, salinity values below 17 can be used to trace this water mass. This is also suggested by field data recorded during EROS21 cruises (Ragueneau *et al.*, 2002). A salinity value below 17 can thus be used to identify water masses which are enriched by nutrients from the river discharge. In these water masses we expect a different behaviour of phytoplankton, compared to open sea waters which gain their nutrients from upwellings and entrainments.

A comparison of the modelled salinity field with the CZCS images of the same period (Barale & Murray, 1995) shows that the high resolution model produces frontal structures with similar scales and positions. The biological model of Gregoire *et al.* (1998) also produces a strong correlation between phytoplankton distributions and the salinity frontal structures. The results of the model and *in situ* data Ragueneau *et al.* (1999) suggest thus that the ecosystem in the regions of low salinity has distinct properties, a fact we will now try to exploit to reduce the complexity of the coupled model. For additional details on the 3-D modelling we refer to Stanev *et al.* (1999).

0-D diagnoses for coupling with a biological model

As suggested by fields data and modelling results, the isohaline of salinity 17 defines the strong front which separates open sea from river-influenced waters. Since we have shown that a high resolution model exhibits much stronger and realistic frontal structures in the region of the Danube River, we suggest using the same model for diagnosis purposes. Since a salinity level of 17 defines an interface between coastal and open sea water masses, one can attempt to model them through a box version approach. Such box models have the advantage of being relatively inexpensive, allowing systematic sensitivity tests in complex biological models. In the second part of the paper (Lancelot *et al.*, 2002*b*), this box model is applied to a specific biological model of the Black Sea, but the method is applicable to any tracer model. To develop a box model, we have to take into account the following elements:

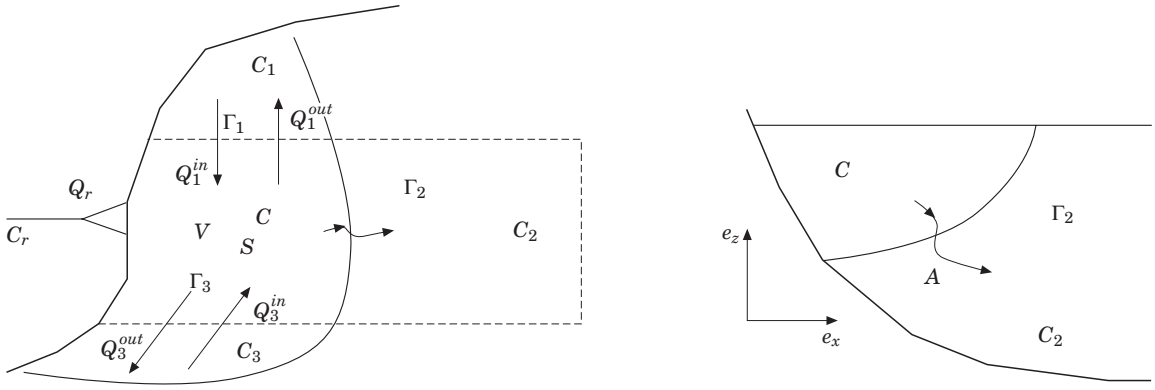

FIGURE 12. Schematic representation of the box model. V is the volume of water considered between fixed latitudes and a moving interface defined by $S=17$. This volume is supposed not to detach from the river mouth, otherwise some lateral mixing exchanges should replace the river input. S is the sea surface delimited by the two latitudes and the intersection with the surface of constant salinity T_2. T_1 is the vertical surface defined by a given northern latitude and its intersection with the isosurface $S=17$. This is the northern, upper limit of the box model. T_2 is the isosurface $S=17$ delimited by the two latitudes and defines the eastern lateral limit of the box model. T_3 is the vertical surface defined by a given southern latitude and its intersection with the isosurface $S=17$. This is the lower, southern limit of the box model. C_r, C_1, C_2, C_3, C is the concentration of a tracer in the river, the northern part, the open sea, the southern part and the plume respectively.

- The water mass of the box model moves and the boundary of the box is therefore not fixed. For mixed layer dynamics, the definition of a water volume whose size changes is classical (e.g. Fasham *et al.*, 1990). According to this definition, the interface moves up and down leaving behind part of the biologically active zone, or entraining water from below. Here, in the river-influenced region, a similar situation occurs when the Danube plume oscillates horizontally in addition to the variations in the mixed layer depth.
- The box volume used to define the plume cannot extend too far. It can't exceed the distance covered by a moving water parcel during a typical biological time scale of, for example, the delay between phytoplankton peaks and zooplankton peaks, otherwise the volume cannot be assumed to be homogeneous (this is one of the basic assumptions of box models).

This suggests that the definition of the box as the total low salinity volume delimited by the surface of salinity 17 is not recommended, since the corresponding volume is relatively large. During the transfer from the river mouth to a distant southern boundary, the biological system could have enough time to evolve, compared to the system near the river mouth.

Integration strategy

We therefore develop the following integration strategy making use of the notations of Figure 12. We first define a fixed box ofi the Danube delta. In this box, we define the box volume to be the volume whose salinity is below 17. This allows to track displacement of the front, but needs to address the problem of inflows and outflows at the northern and southern fixed boundaries.

The choice of fixed zonal boundaries can a priori be supported by the fact that (particularly south of the Danube) the signature of the low salinity is relatively narrow, and actually evolves smoothly into a coastal salinity front (Figure 4).

In the appendix we show how the actual integration over the moving and open 0-D box can be obtained mathematically and where additional hypotheses are needed to close the formulation in terms of integrated variables only: one assumes for example that the total integral of source term can be retrieved by applying the local source law P^C to the average concentrations. This is only true when interaction laws are linear or if the laws have been adapted (through a specific calibration) to represent large scale interactions rather than local, physiologically-based interactions. Similarly, the sea-surface interactions generally depend on the evolution of the constituent in the water mass itself. We must assume that the integral of the sea-surface exchange can be expressed in terms of the average concentration of the tracer [Equation (22)]. The same hypotheses apply to the fluxes across the fixed boundaries Γ_1 and Γ_3. Here one should bear in mind that these fluxes are dominated by advective fluxes whose integration can be written as the product of the water mass flow and concentrations of inflow or outflow [equations (23) and (24)].

Based on such assumptions, in order to be able to force the box model, one must at least have either field data or diagnosed values from the 3-D model for the following parameters: river discharge Q_r in $m^3\,s^{-1}$ into the sea, the water inflow Q_1^{in} into the volume coming from the north, the outflow Q_1^{out} to the north on the northern boundary, the inflow from the south Q_3^{in}, the outflow to the south Q_3^{out}, the sea surface flux counted positive upwards F^C, the inflow concentrations in the north C_1 and the south C_3.

Providing such parameters are known, based on our assumptions and omitting notations for averages, the evolution of the average concentration in the box is governed by:

$$V\frac{dC}{dt}+C\frac{dV}{dt}=V\,P^C+Q_rC_r+Q_1^{in}C_1-Q_1^{out}C+Q_3^{in}C_3-Q_3^{out}C-F^CS+D \quad (1)$$

where

$$D=-\int_{\Gamma_2}\boldsymbol{n}\cdot((v-v_\Gamma)C-\boldsymbol{K}\cdot\nabla C)\,d\Gamma_2 \quad (2)$$

is the total diffusion flux across the moving interface and C the average concentration of the tracer in the volume V.

D must also be parameterized. Unlike fluxes across the fixed boundaries, advection is not dominant (by construction, the surface is a material surface and no advection fluxes cross it) and the parameterization will be a diffusion-like flux. This requires the definition of an equivalent diffusion coefficient A. The calculation of the latter is based on an equivalent diffusion flux formulation for salinity or temperature. Its actual value for the total diffusion flux D can be diagnosed thanks to the physical high resolution model, integrating the actual salinity fluxes from Equation (2) and calculating A as follows:

$$A=\frac{D}{S_2-S} \quad (3)$$

where S and S_2 are the averaged salinities (or temperatures) from the model.

Combination of equations (1)–(3) gives:

$$V\frac{dC}{dt}+C\frac{dV}{dt}=VP^C+Q_rC_r+Q_1^{in}C_1-Q_1^{out}C+Q_3^{in}C_3-Q_3^{out}C-F^CS+A(C_2-C) \quad (4)$$

In particular, mass conservation integrated over V can be retrieved by setting $C_\star=1$; $P^C=0$; $F^C=0$ which gives

$$\frac{dV}{dt}=Q_r+Q_1^{in}-Q_1^{out}+Q_3^{in}-Q_3^{out} \quad (5)$$

Finally, this leads to the equation governing the average concentration in the box:

$$\frac{dC}{dt}=P^C+\frac{Q_r}{V}(C_r-C)+\frac{Q_1^{in}}{V}(C_1-C)+\frac{Q_3^{in}}{V}(C_3-C)-F^C\frac{S}{V}+\frac{A}{V}(C_2-C) \quad (6)$$

which is easily implemented into an existing 0-D code, as long as Q_1^{in}, Q_3^{in}, Q_r, V, C_r, C_1, C_2, C_3 are provided by the 3-D model or data.

Application to the Danube river influenced region

Figure 13 shows the evolution of the water volume of salinity below 17, defined by the moving lateral boundary and the fixed north and southern boundaries. The spring increase, attributable to the high Danube discharge (Qd), is clearly visible.

Figure 14 shows the evolution of salinity concentrations over time. Basically open sea salinity remains constant while inflowing waters are clearly influenced by freshwater inputs from the north, the Dnepr and Dnestr discharges.

As regards temperature (Figure 15), the seasonal cycle is clear, but so too is the input of warmer waters from the north ($QT1/Q1$), which do not result from the mixing of open shelf waters and plume waters, since their temperature values are higher than those of plume (T) and shelf waters ($T2$). This is most likely due to the heating of the water masses in the shallower northern region in spring and summer.

The evolution of inflowing water fluxes (Figure 16) shows the relatively large amplitude of these fluxes. One must however bear in mind, in view of Equation (6), that the important parameter for the evolution of the box average concentration C is not Q^{in} but Q^{in} (C^{in}–C), which may be strongly influenced by the way the tracer concentration of the inflowing waters C^{in} is assessed.

The high resolution 3-D model diagnostics for these quantities indicate that the model's precision is limited by several factors:

- A is different when the calculation is based on salinity or heat fluxes, with differences larger than 100%.
- Values of C_2, C_1 and C_3 are highly subjective, especially when assuming, for example, that C_3 is a mixing of C_2 and C. This would amount to a change the water inflow of Q_3.

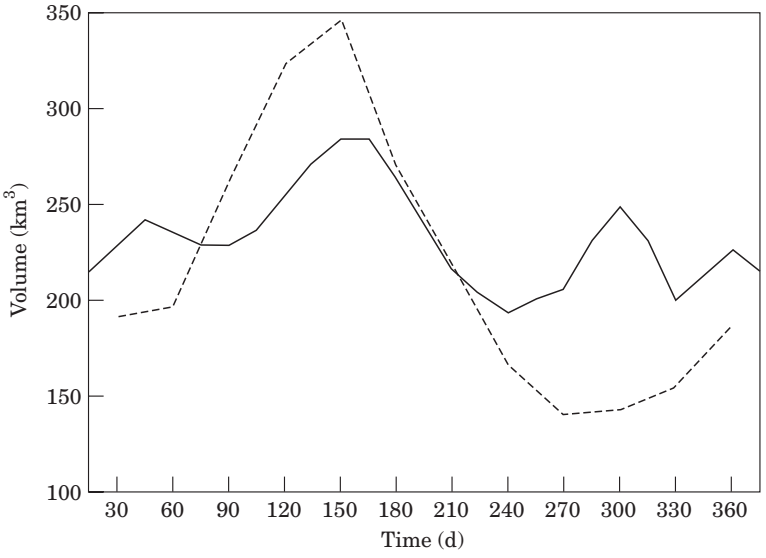

FIGURE 13. Seasonal evolution of the volume V (——, in km^3) and of the Danube discharge (– – –, Qd).

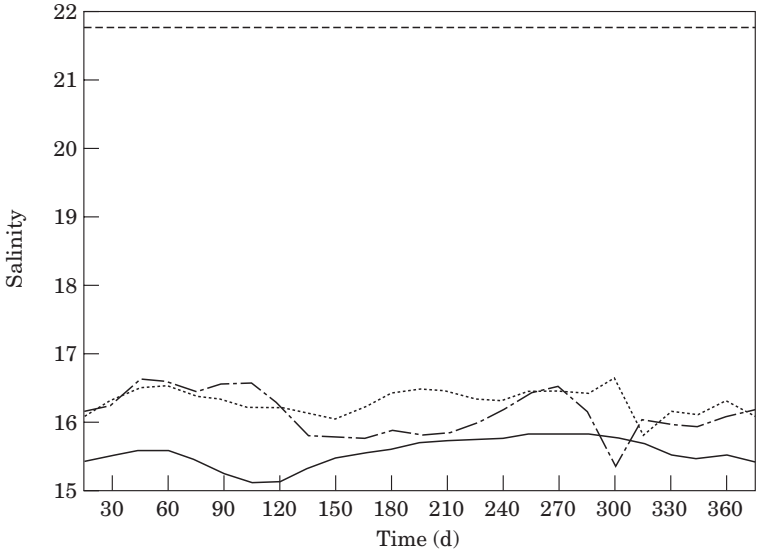

FIGURE 14. Seasonal evolution of salinity values in the open sea ($S2$, highest salinity around 21·8), the plume (S, lowest salinity around 15·5), the inflow from the north ($QS1 = Q1$) and the inflow from the south ($QS3 = Q3$). The last two are evaluated by dividing the total salt inflow by the water inflow. (– – –) $S2$; (——) S; (— - —) $Q1$ and (------) $Q3$.

- Only volume-averaged temperatures are available, which may be too approximate for use in functions limiting growth rate that are used in biological models. These may react to high temperatures in the surface but not to lower temperatures below the thermocline.

Unfortunately, the mixing coefficient A and the possible mixing of C_2 and C for inflow values C_1 and C_3 may be different for different state variables. This state of affairs may not be overcome. Indeed, the diagnosis of the mixing in the 3-D model can only be performed on variables of the 3-D model. We must thus make some assertions of how these coefficients, based on temperature and salinity fields, can be extended to biological variables. This ultimately implies sensitivity studies in the 0-D model, in which these coefficients should be systematically changed and responses compared. The amplitude of the uncertainty regarding such coefficients can be

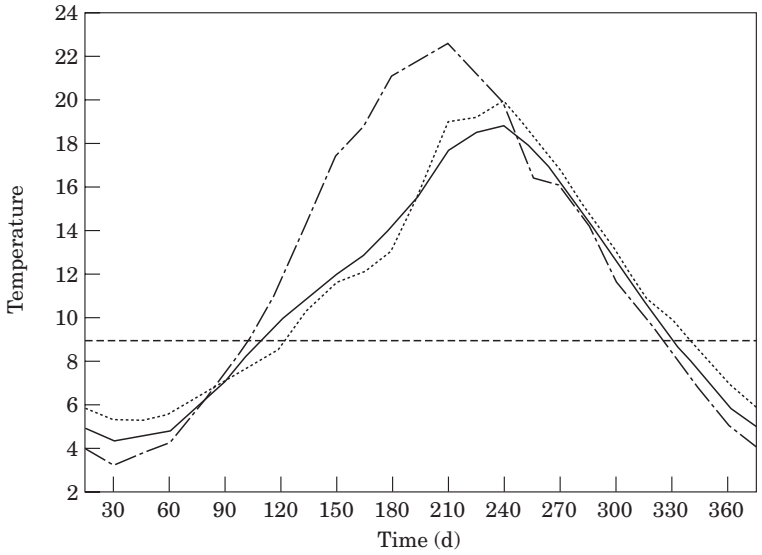

FIGURE 15. Seasonal evolution of temperature in the open sea ($T2$, almost constant), the plume (T), the inflow from the north ($QT1 = Q1$ with highest temperatures) and the inflow from the south ($QT3 = T3$). The last two are evaluated by dividing the total temperature inflow by the water inflow. (– – –) $T2$; (— - —) T; (·····) $QT3/Q3$ and (——) $QT1/Q1$.

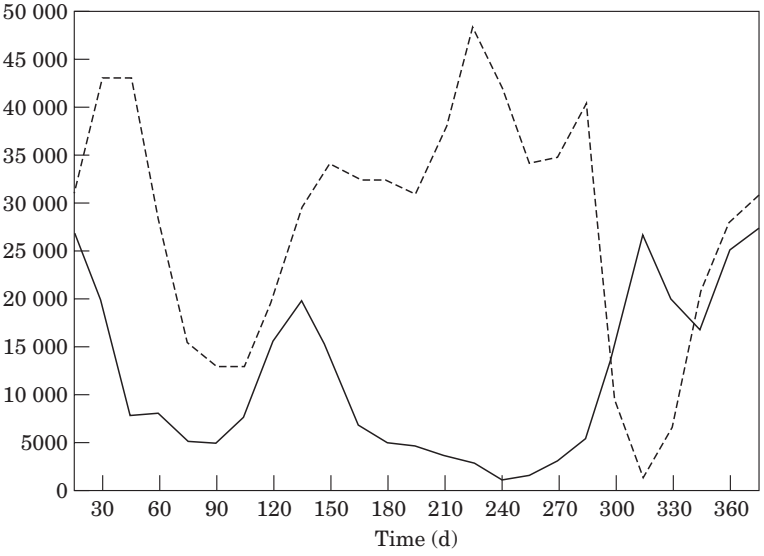

FIGURE 16. Seasonal evolution of Q_1^{in} (lower curve, in $m^3\ s^{-1}$) and Q_3^{in}. (– – –) $Q1$ and (——) $Q3$.

assessed by calculating the different mixing coefficients for temperature and salinity based on direct calculations in the 3-D model. An alternative would be to calibrate such coefficients in such a way that the 0-D model applied to salinity and temperature yields a response which is the exact average of the 3-D model response.

In other words, if we assume the inflow values C_1 and C_3 are a mixing of open sea waters C_2 and the modelled values C we obtain

$$C_1 = \alpha_1 C_2 + (1-\alpha_1) C \tag{7}$$

$$C_3 = \alpha_3 C_2 + (1-\alpha_3) C \tag{8}$$

In this case the evolution reads

$$\frac{dC}{dt} = P^C + \frac{Q_r}{V}(C_r - C) + \left(\alpha_1 \frac{Q_1^{in}}{V} + \alpha_3 \frac{Q_3^{in}}{V} + \frac{A}{V}\right)(C_2 - C) - F^C \frac{S}{V} \tag{9}$$

and we see that the evolution reduces to

$$\frac{dC}{dt} = P^C + \frac{Q_r}{V}(C_r - C) + \frac{\tilde{A}}{V}(C_2 - C) - F^C\frac{S}{V} \quad (10)$$

with the equivalent exchange coefficient

$$\tilde{A} = \alpha_1\frac{Q_1^{in}}{V} + \alpha_3\frac{Q_3^{in}}{V} + \frac{V}{A} \quad (11)$$

which can be calibrated so that the time evolutions of S or T correspond to those of the 3-D model.

$$\tilde{A} = \left(V\frac{dS^{3D}}{dt} - Q_r(0 - S^{3D}) + F^C S\right)\frac{1}{S_2^{3D} - S^{3D}} \quad (12)$$

This can also be considered as an alternate method to compute the equivalent mixing coefficient $\tilde{A}$ which mixes zero water salinity waters with open sea waters so that the salinity to which the time evolution tends in absence of a surface forcing is

$$S = \frac{\tilde{A}}{\tilde{A} + Q_r}S_2 \quad (13)$$

which allows to have a rough estimate of A depending on the river discharge and the observed average plume salinity.

$$\tilde{A} = \frac{S}{S_2 - S}Q_r \quad (14)$$

Finally, we observe that two time scales intervene $\frac{V}{Q_r}$ and $\frac{V}{A}$ corresponding to the residence time of river waters and open sea waters in the volume over a period of 100 days.

From the detailed analysis shown here, it also appears that for the development of the volume-integrated 0-D model the best response can be expected when the direction of the main current does not change. If, for example, the current flowed from north to south, integration would be performed on the northern boundary defined by $S = 17$ and a fixed boundary in the south. In this case, Q_1^{in} and Q_3^{in} would be zero, since the northern boundary follows the fluid while the southern boundary only has an outflow. Also, all hypotheses on inflow concentrations could be dropped; the southern boundary would be chosen so that the biological time scale in this box is small compared to the advective time scale across the box. The model would thus only have a single parameter based on a strong hypothesis, i.e. coefficient A. Unfortunately, in the case of the Black Sea and the Danube, not only does the current direction change, from southward in winter to northward in summer, but the salinity boundary defined by $S = 17$ may be influenced by other rivers. This makes it difficult to distinguish between Danube waters and Dnepr-Dnestr waters using only salinity values.

In the 3-D model, plume behaviour is observed in the salinity, but not in the temperature. Using temperature to diagnose the diffusion coefficient was not reliable, since the temperature within the plume is not homogeneous and the diffusion fluxes at the boundary are generally not related to the temperature difference between the average temperature in the plume and the open sea. The difference in behaviour also occurs because the forcing in the area is too different for T and S, (source point for S and homogeneously distributed source for T at the sea surface).

From the evolution of the inflow temperatures (Figure 15) and salinities (Figure 14), it is also observed that, as regards temperature, inflowing waters are not a simple mixing between open sea waters and the 0-D variable, since the water masses flowing in may have higher temperatures. This also appears in the diagnosed diffusion coefficient for the temperature calculated by inversion of Equation (12) for temperature. Indeed, negative equivalent diffusion coefficients indicate that temperature increases within the plume, even if its temperature is higher than that of deep waters, because some inflow from the north or south brings warmer waters into the system. For salinity the situation is different, since the Danube is the major fresh water source on the shelf. It means that situations where the main currents brings low salinity waters into the plume are rare and correspond to situations where the Dnepr and Dnestr have discharged large amounts of fresh waters arriving in the Danube region when discharges are already decreasing. For salinity, the equivalent diffusion coefficient is thus predominantly positive, but not so for temperature. Similarly, one may expect negative values of this equivalent diffusion coefficient for biological components in situations where the biosystem in the north of the Danube region has a distinct composition from both the open sea and the Danube region. Mathematically, this corresponds to situations where a_1 of Equation (7) is negative or larger then 1, indicating that the inflow value C_1 does not result simply from mixing the open sea value C_2 with the Danube plume value C.

Some estimates of diffusion coefficients A, necessary to close the system, show large spreading of the different estimates (Figure 17). Estimates differ

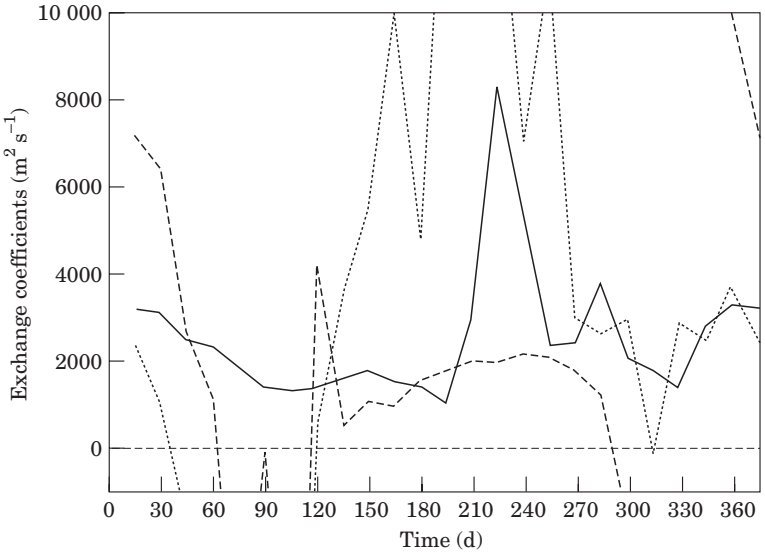

FIGURE 17. Seasonal evolution of exchange coefficient A. AS is based on the salt diffusion flux according to Equation (3), AT similarly but based on the 3-D heat flux across the moving interface. AS1 is diagnosed from the evolution of the model averaged salinities; the corresponding values for temperature are not shown because they lie outside the range specified here, with mostly negative values. (——) AS; (------) AS1 and (– – –) AT.

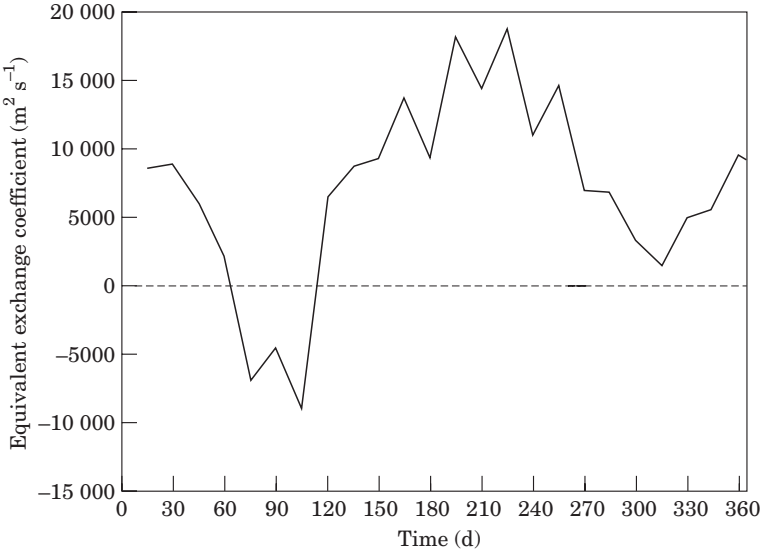

FIGURE 18. Seasonal evolution of the equivalent diffusion coefficient $\tilde{A}$ (in m^3 s^{-1}) based on the salinity Equation (12). (——) AT.

already for temperature and salinity when they are calculated directly from the total diffusive flux across the moving interface. They differ even more when evaluated from the inversion of the time evolution equation (calculating A which provides the 3-D model averaged temperature when using the 0-D model). This demonstrates that the box model can only be applied to variables which have plume-like behaviour.

Since hypotheses on the inflow concentrations of such variables must be formulated, one can also try to estimate equivalent diffusion coefficients, also taking into account some mixing of the inflow parameters [Equation (12)]. Figure 18 shows the seasonal evolution of the equivalent diffusion coefficient for salinity. The coefficient for temperature is not shown, since large variations and negative values are diagnosed, indicating a non-mixing behaviour of temperature, which is actually due to an advective heat inflow.

The values of the diagnosed diffusion coefficient give an idea of the range of values these coefficients

can take, depending on the way the inflowing water masses carry mixed water masses from the Danube, Dnepr, Dnestr and the open sea.

Conclusions and discussions

We have shown that both coarse and high resolution models give a general circulation pattern compatible with classical views of circulation in the Black Sea.

Of these two models, the high resolution model has more marked fronts and greater internal variability. For the Danube region, both models simulate a reversal of the current during the summer season. The high resolution model results are better suited for the preparation of a 0-D coupled model: as was shown, only the high resolution model adequately resolves the frontal dynamics.

The 0-D model is certainly improved by using information from a 3-D model, but it still has some inherent limitations which must be recognized. The advantage of the 0-D model is of course its simplicity for a systematic sensitivity study with respect to biological parameters and the physical parameters of in-flow values and inflow mixing coefficients. If such sensitivity studies show that a change in the Danube river inflow has stronger impacts on the system response than the values of these coefficients, one can use the 0-D model to analyse the effect of human activity through the Danube discharge. However, if sensitivity is too high, a more complex model becomes indispensable in order to do away with the hypotheses underlying the calculation of these parameters. As shown in the companion paper of Lancelot *et al.* (2002*b*), the model shows that the effect of the changing conditions in the Danube leads to stronger signals than due to changes in the exchange coefficient A of the 0-D model. This means that the resulting 0-D model can be used as a first approach to study the Danube river discharge effects, provided the exchange coefficients are taken in a reasonable range, as was effectively calculated by the 3-D model, and that the inflow conditions are well known.

When the mixing ratios of the inflowing waters are not known (reflected by uncertainties of the mixing values α), simulations can be performed, using mixing ratios for biological components similar to those of salinity. This shows that the biological model's response to such changes has a similar amplitude to changes in the Danube river discharge, indicating that the inflow conditions from the open sea are of major importance for the biological model at the mouth of the Danube.

Assuming that the problem of the inflow conditions can be solved thanks to a nesting technique, a further improvement of any model must then be achieved by the use of synoptic atmospheric data rather than climatological data.

Acknowledgements

The development of the GHER model has been funded for several years by the European Union. The work presented here is part of the EU EROS21 project in the ELOISE framework (contract EVSV-CT94-0501 and associated contract IC20-CT96-0065). This is publication No. 184 of ELOISE.

The National Fund for Scientific Research (Belgium) has given two authors (J M B and M G) the opportunity to be actively involved in oceanographic research.

IBM Belgium, IBM Europe and IBM International Foundation provided supercomputer assistance, most recently in the scope of the ERP-SALMON project (Sea Air Land Modelling Operational Network).

The German Alexander von Humboldt Stiftung awarded a grant to two authors which allowed them to write part of the present version of the manuscript, and to acquire modelling expertize in the Black Sea.

References

Altman, E. N. & Kumish, N. I. 1986. Interannual and seasonal variability of the Black Sea fresh water balance. *Trudi Gos. Oceanographic Institute* **145,** 3–15 (in Russian).

Barale, A. & Murray, C. 1995 The surface colour field of enclosed marine basins: Pigment patterns of the Black Sea. *Remote Sensing Reviews* **12,** 61–82.

Beckers, J.-M. 1991 Application of a 3D model to the Western Mediterranean. *Journal of Marine Systems* **1,** 315–332.

Beckers, J.-M. 1994 On destabilizing implicit factors in discrete advection–diffusion equations. *Journal of Computational Physics* **111,** 260–265.

Beckers, J.-M. & Deleersnijder, E. 1993 Stability of a FBTCS scheme applied to the propagation of shallow-water inertia-gravity waves on various space grids. *Journal of Computational Physics* **108,** 95–104.

Chao, S.-Y. & Boicourt, W. C. 1986 Onset of estuarine plume. *Journal of Physical Oceanography* **16,** 2137–2214.

Deleersnijder, E. & Beckers, J.-M. 1992 On the use of the σ-coordinate system in regions of large bathymetric variations. *Journal of Marine Systems* **3,** 381–390.

Delhez, E. 1998 Macroscale ecohydrodynamic modeling in the northwest European continental shelf. *Journal of Marine Systems* **16,** 171–190.

Demirov, E. K. 1994 Numerical modelling of the Black Sea eigen-oscillations on a curvilinear boundary fitted coordinate system. *Dynamics of Atmosphere and Ocean* **21,** 83–103.

Fasham, M., Ducklow, H. & McKelvie, S. 1990 A nitrogen-based model of the plankton dynamics on the oceanic mixed layer. *Journal of Marine Research* **48,** 591–639.

Filippov, D. M. 1968 *Circulation and water composition of the Black Sea*. Nauka, Moscow, 136 pp.

Gamsakhurdiya, G. R. & Sarkisyan, A. 1976 Diagnostic calculations of the current velocities in the Black Sea. *Oceanology* **15,** 164–167 (in Russian).

Gregoire, M., Beckers, J.-M., Nihoul, J. & Stanev, E. 1997 Coupled hydrodynamic ecosystem model of the Black Sea at basin scale. Model description and first results. In *Sensitivity to change: Black Sea, Baltic Sea and North Sea*, volume 27 of NATO ASI Series (Ozsoy, E. & Mikaelyan, A., eds) Kluwer Academic, pp. 487–499.

Gregoire, M., Beckers, J.-M., Nihoul, J. & Stanev, E. 1998 Reconnaissance of the main Black Sea's ecohydrodynamics by means of a 3D interdisciplinary model. *Journal of Marine Systems* **16,** 85–105.

Hickey, B., Pietrafesa, L., Jay, D. & B.W.C. 1998 The Columbia river plume study: subtidal variability in the velocity and salinity fields. *Journal of Geophysical Research* **103,** 10339–10368.

Ivanov, L., Besiktepe, S. & Ozsoy, E. 1997 The Black Sea cold intermediate layer. In *Sensitivity to change: Black Sea, Baltic Sea and North Sea*, Volume 27 of NATO Asi Series (Ozsoy, E. & Mikaelyan, A., eds). Kluwer Academic, pp. 253–264.

Lancelot, C., Martin, J.-M., Panin, N. & Zaitsev, Y. 2002*a* The north-western Black Sea: a pilot site to understand the complex interactions between human activities and the coastal environment. *Estuarine, Coastal and Shelf Science* **54,** 279–283.

Lancelot, C., Staneva, J., Van Eeckhout, D., Stanev, E. & Beckers, J.-M. 2002*b* Modelling the Danube river influenced North-Western continental shelf of the Black Sea: Part II: Modelling the impact of the human forcing on the ecological functioning. *Estuarine, Coastal and Shelf Science* **54,** 473–499.

Nihoul, J. 1998 Modelling marine ecosystems as a discipline in earth science. *Earth Science Review* **44,** 1–13.

Nihoul, J. C. J., Deleersnijder, E. & Djenidi, S. 1989 Modelling the general circulation of shelf seas by 3D k–ε models. *Earth Science Reviews* **26,**163–189.

Nomérange, P. & Beckers, J.-M. 1999 A nesting procedure for a 3D primitive equation ocean model. GHER Report, University of Liège.

Oguz, T., Besiktepe, S., Basturk, O., Salioglu, I., Aubrey, D. G., Balci, A., Demirov, E., Diaconu, V., Dorogan, L., Duman, M., Ivanov, L., Konovalov, S., Stoyanov, A., Turgul, S., Vladimirov, V. & Hilmaz, A. 1993 Comsblack 92, a physical and chemical intercalibration workshop. 15–29 January 1993, Erdemli, Turkey. Intergovernmental Oceanographic commission Workshop Report.

Oguz, T., Malanotte-Rizzoli, P. & Aubrey, D. 1995 Wind and thermohaline circulation of the Black Sea driven by yearly mean climatological forcing. *Journal of Geophysical Research* **100,** 6845– 6863.

Oguz, T. E. & Malanotte-Rizzoli, P. 1996 Seasonal variability of wind and thermohaline driven circulation in the Black Sea. *Journal of Geophysical Research* **101,** 16585–16599.

Oguz, T. E., Ozsoy, E., Latif, A., Sur, H. & Unluata, U. 1990 Modeling of hydrographically controlled exchange flow in the Bosphorus strait. *Journal of Physical Oceanography* **20,** 945–965.

Ozsoy, E., Unluata, U. & Top, Z. 1993 The evolution of Mediterranean water in the Black Sea: interior mixing and material transport by double diffusive intrusions. *Progress in Oceanography* **31,** 275–320.

Ragueneau, O., Lancelot, C., Egorov, V., Cociasu, A., Vervlimmeren, J., Daoud, N., Rousseau, V., Popovitchev, V., Brion, N., Popa, L., Kraster, A. & Goeyens, L. 2002 Biogeochemical transformation of inorganic nutrients in the Danube-north-western Black Sea mixing zone. *Estuarine, Coastal and Shelf Science* **54,** 321–336.

Simonov & Altman (eds) 1991 *Hydrometeorology and hydrochemistry of the USSR seas*, volume IV The Black Sea. Gidrometeoizdat, 430 pp.

Sorokina, A. 1974 *Reference book on the Black Sea climate*. Gidrometeoizdat, Moscow, 406 pp.

Stanev, E., Beckers, J.-M., Lancelot, C., Le Traon, P., Staneva, J., Peneva, P. & Gregoire, M. 2002 Coastal-open ocean exchange. Black Sea examples from survey, satellite data and modeling. *Estuarine, Coastal and Shelf Science* **54,** 601–620.

Stanev, E. V. 1988 Numerical study on the Black Sea circulation. Technical report, Mitteilungen des Instituts für Meereskunde der Universität, Hamburg, 232 pp.

Stanev, E. V. 1990 On the mechanisms of the Black Sea circulation. *Earth-Science Review* **28,** 285–319.

Stanev, E. V. & Beckers, J.-M. 1998 Barotropic and baroclinic oscillations in strongly stratified ocean basins. Numerical study of the Black Sea. *Journal of Marine Systems* **19,** 65–112.

Stanev, E. V. & Beckers, J.-M. 1999 Numerical simulations of seasonal and interannual variability of the Black Sea thermohaline circulation. *Journal of Marine Systems* **22,** 241–267.

Stanev, E. V., Roussenov, V. M., Rachev, N. & Staneva, J. V. 1995 Seasonal response to atmospheric variability. Model study for the Black Sea. *Journal of Marine Systems* **6,** 241–267.

Stanev, E. V., Truhchev, D. & Roussenov, V. 1988 *The Black sea circulation and numerical modelling of the Black Sea currents*. Sofia University Press, 240 pp.

Appendix

To show how the box model can by established and where the strong hypotheses are made, we start from the conservation equation for any tracer C:

$$\frac{\partial C}{dt}+\nabla\cdot(\boldsymbol{v}C)=\nabla\cdot(\boldsymbol{K}\cdot\nabla C)+P^C \qquad (15)$$

where $\boldsymbol{v}$ is the 3-D vector field, $\boldsymbol{K}$ is the anisotropic diffusion tensor and P^C the local source term of the tracer (which may depend on other variables).

Integration over the variable volume yields

$$\int_V\frac{\partial C}{\partial t}dV=-\int_V\nabla\cdot(\boldsymbol{v}C-\boldsymbol{K}\cdot\nabla C)\,dV+\int_V P^C dV \qquad (16)$$

For a volume moving with the velocity fields $\boldsymbol{v}_V$, the Leibnitz rule can be applied:

$$\begin{aligned}\int_V\frac{\partial C}{\partial t}dV&=\frac{\partial}{\partial t}\left(\int_V CdV\right)-\int_V\nabla\cdot\boldsymbol{v}_V CdV\\&=\frac{\partial}{\partial t}\left(\int_V CdV\right)-\int_\Gamma\boldsymbol{v}_\Gamma\cdot\boldsymbol{n}Cd\Gamma\end{aligned} \qquad (17)$$

where T is the total surface surrounding the volume V, so that

$$\begin{aligned}&\frac{\partial}{\partial t}\left(\int_V CdV\right)-\int_\Gamma\boldsymbol{v}_\Gamma\cdot\boldsymbol{n}Cd\Gamma=\\&-\int_{\Gamma_1}\boldsymbol{e}_y\cdot(\boldsymbol{v}C-\boldsymbol{K}\cdot\nabla C)\,d\Gamma_1+\int_{\Gamma_3}\boldsymbol{e}_y\cdot(\boldsymbol{v}C-\boldsymbol{K}\cdot\nabla C)\,d\Gamma_3\\&-\int_{\Gamma_2}\boldsymbol{n}\cdot(\boldsymbol{v}C-\boldsymbol{K}\cdot\nabla C)\,d\Gamma_2+\int_S\boldsymbol{e}_z\cdot(\boldsymbol{K}\cdot\nabla C)\,dS\\&+\int_S-C\boldsymbol{n}\cdot\boldsymbol{v}dS+\int_V P^C dV+Q_rC_r\end{aligned} \qquad (18)$$

The second term on the left hand side provides the correction of the balance. This is due to the fact that changes in volume are such that at each point on the surface Γ the points of the surface move with velocity $\boldsymbol{v}_\Gamma$, whose projection onto the normal $\boldsymbol{n}$ to the surface is needed to evaluate the ow across the moving surface.

Since Γ is composed of fixed boundaries Γ_1, Γ_3, coasts and rivers, the correction only arises from the moving sea surface and the interface Γ_2. The sea surface is a material surface of the fluid, which means that its elements are actual water parcels which move with the fluid: $\boldsymbol{v}\cdot\boldsymbol{n}=\boldsymbol{v}_\Gamma\cdot\boldsymbol{n}$ on the sea surface. In this case, the integration yields

$$\begin{aligned}\frac{d}{dt}\left(\int_V C dV\right) &= -\int_{\Gamma_1}\boldsymbol{e}_y\cdot(\boldsymbol{v}C-\boldsymbol{K}\cdot\nabla C)\,d\Gamma_1\\ &\quad+\int_{\Gamma_3}\boldsymbol{e}_y\cdot(\boldsymbol{v}C-\boldsymbol{K}\cdot\nabla C)\,d\Gamma_3\\ &\quad-\int_{\Gamma_2}\boldsymbol{n}\cdot((\boldsymbol{v}-\boldsymbol{v}_{\Gamma_2})C-\boldsymbol{K}\cdot\nabla C)\,d\Gamma_2+\int_S\boldsymbol{e}_z\cdot(\boldsymbol{K}\cdot\nabla C)\,dS\\ &\quad+\int_V P^C dV+Q_r C_r \qquad (19)\end{aligned}$$

To express the different parts as functions of the averaged values, certain approximations must be performed:

$$\int_V C dV = V\bar{C} \qquad (20)$$

$$\int_V P^C dV = VP^C(\bar{C}) \qquad (21)$$

$$\int_S -\boldsymbol{e}_z\cdot(\boldsymbol{K}\cdot\nabla C)\,dS = SF^C(\bar{C}) \qquad (22)$$

$$\int_{\Gamma_3}\left(\boldsymbol{e}_y\cdot\boldsymbol{v}C-\bar{\kappa}_T\frac{\partial C}{\partial y}\right)d\Gamma_3 = Q_3^{in}\bar{C}_3-Q_3^{out}\bar{C} \qquad (23)$$

$$\int_{\Gamma_1}-\left(\boldsymbol{e}_y\cdot\boldsymbol{v}C-\bar{\kappa}_T\frac{\partial C}{\partial y}\right)d\Gamma_1 = Q_1^{in}\bar{C}_1-Q_1^{out}\bar{C} \qquad (24)$$

$$v_{\Gamma 2}\cdot n = v\cdot n \qquad (25)$$

Equation (20) defines the calculated 0-D variable as the average concentration in the volume being considered. This is not a hypothesis but a definition, whereas the remaining expressions need certain hypotheses to close the mathematical system: indeed, Equation (21) assumes for example that the total integral of the source term can be retrieved by applying the local source law to the average concentrations. This is only true when the interaction laws are linear or if the laws have been adapted (through specific calibration) to represent large scale interactions rather than local, physiologically-based interactions. The last condition assumes that the interface between the two parts is a material surface. Otherwise, the contribution of the advective part is to be formulated in terms of entrainment-detrainment Q_e, Q_d. The sea-surface interactions are generally dependent on the evolution of the constituent in the water mass itself, and again, we must assume that the integral of the sea-surface exchange can be expressed in terms of the average concentration of the tracer [Equation (22)]. The same hypotheses apply to the fluxes across the fixed boundaries T_1 and T_3. Here we take into account that these fluxes are dominated by advective fluxes, whose integration can be written as the product of the water mass and in or outflow concentrations [equations (23) and (24)].